ISSN 1023-1935, Russian Journal of Electrochemistry, 2018, Vol. 54, No. 6, pp. 486–492. © Pleiades Publishing, Ltd., 2018.
Original Russian Text © A.I. Ivanov, V.A. Kolotygin, M.V. Patrakeev, A.A. Markov, S.I. Bredikhin, V.V. Kharton, 2018, published in Elektrokhimiya, 2018, Vol. 54, No. 6, pp. 561–569.

Oxygen Nonstoichiometry and Transport Properties of Mixed-Conducting $Ce_{0.6-x}La_{0.4}Pr_xO_{2-\delta}$[1]

A. I. Ivanov[a], *, V. A. Kolotygin[a], M. V. Patrakeev[b], A. A. Markov[b], S. I. Bredikhin[a], and V. V. Kharton[a]

[a] *Institute of Solid State Physics, Russian Academy of Sciences, Chernogolovka, Moscow oblast, 142432 Russia*
[b] *Institute of Solid State Chemistry, Ural Branch, Russian Academy of Sciences, Yekaterinburg, 620990 Russia*
**e-mail: aliv@issp.ac.ru*

Received September 5, 2017; in final form, January 12, 2018

Abstract—The oxygen nonstoichiometry and electrical conductivity of fluorite-type solid solutions $Ce_{0.6-x}La_{0.4}Pr_xO_{2-\delta}$ (x = 0.1–0.2) were studied in the oxygen partial pressure range 10^{-19}–0.35 atm at 1023–1223 K. It was confirmed that the $Pr^{4+/3+}$ and $Ce^{4+/3+}$ redox pairs, which determine the concentration of p- and n-type electron charge carriers, play the dominant roles under oxidizing and reducing conditions, respectively. The conductivity vs. charge carrier concentration dependencies in these conditions are almost linear. Increasing praseodymium content leads to a substantially higher hole conductivity and an expanded range of the oxygen nonstoichiometry variations at high oxygen partial pressures. Under reducing conditions when praseodymium cations become trivalent opposite trends are observed on doping.

Keywords: doped ceria, oxygen vacancies, mixed conductivity, defect formation, thermodynamic stability

DOI: 10.1134/S1023193518060058

INTRODUCTION

Currently, fluorite-like solid solutions $(Ce,Ln)O_{2-\delta}$, where Ln is the rare earth metal cation, are used as components of solid oxide fuel cells (SOFCs), membranes for oxygen generators, electrochemical sensors, and catalysts of oxidation [1–10]. The $Ce_{1-x}Pr_xO_{2-\delta}$ system is of significant practical and scientific interest due to the wide oxygen homogeneity region in combination with mixed ion-electron conductivity, high oxygen exchange rate, and thermodynamic stability during redox cycling [7, 9–17]. According to the data of [3, 11–14], the main mechanism of defect formation in $Ce_{1-x}Pr_xO_{2-\delta}$ and their structural analogs is the formation of oxygen vacancies. At high oxygen partial pressures ($p(O_2)$), the vacancies are statistically distributed in the oxygen sublattice, and a transition to the region of low $p(O_2)$ can lead to the formation of associates of defects of various types and ordering of the lattice [3, 11, 13, 14, 18–20]. The electron transport in these systems is performed by means of polarons of small radius between the Pr^{3+}/Pr^{4+} and Ce^{3+}/Ce^{4+} pairs, which dominate in the oxidation and reduction regions, respectively [13, 14, 17, 21, 22]. The double-doped systems, in particular, $(Ce,La,Pr)O_{2-\delta}$ can be used as electrochemically active protective layers in SOFCs [17]. The presence of praseodymium cations provides electron transport under the cathode (oxidative) conditions of SOFCs and increases the catalytic activity in reactions involving molecular oxygen. On the other hand, partial replacement of cerium with lanthanum (40 at %) near the solubility limit in CeO_2 [23] provides high chemical stability [24–28].

The present work is a continuation of our previous study [17]; the goal of this study was to analyze the oxygen nonstoichiometry of $Ce_{0.6-x}La_{0.4}Pr_xO_{2-\delta}$ (x = 0.1–0.2) and evaluate the dependences of the transport properties on the concentration of oxygen vacancies over a wide range of oxygen pressures at 973–1223 K.

EXPERIMENTAL

The single-phase powders of $Ce_{0.6-x}La_{0.4}Pr_xO_{2-\delta}$ for studying the oxygen nonstoichiometry were obtained using the glycine-nitrate method; the synthesis conditions were described in detail in [17]. The X-ray diffraction (XRD) analysis was performed on a Siemens D-500-Braun X02-1787 diffractometer (Siemens, Germany) (CuK_α radiation, step 0.02°, 20° ≤ 2θ ≤ 90°) at room temperature. The XRD patterns were processed and crystal lattice parameters deter-

[1] Presented at the IV All-Russian Conference "Fuel Cells and Fuel Cell based Power Plants" (with international participation) June 25–29, 2017, Suzdal, Vladimir region.

mined using the PowderCell program package (version 2.4). The changes in oxygen nonstoichiometry were measured by coulometric titration in the range of $p(O_2)$ 10^{-19}–0.35 atm at $T = 1023$–1223 K at a step of 50 K in the CO_2–CO–O_2 gas system; the technique and equipment were described in [29]. As the reference oxygen content we used $\delta = 0.2 + x/2$, which corresponds to the nominal degree of oxidation of cerium and praseodymium 4+ and 3+, respectively. It was assumed that this state corresponds to an inflection on the titration isotherms, which takes place when the dominant equilibrium of defects changes, and the exact value of the corresponding oxygen partial pressure at 1223 K was determined from the extremum of the derivative $\partial\delta/\partial(\log p(O_2))$. The point with the thus determined coordinates ($p(O_2)$, T, δ) was used for fitting the results of coulometric titration to the absolute values of nonstoichiometry. The gas-tight ceramics for studying the electric properties was pressed in the form of disks with a diameter of 27 mm and a thickness of 2.5–3 mm at ~100 MPa and sintered at 1723 K for 10 h in air with an average heating/cooling rate of no more than 2.5 K/min. The samples were cut out of the sintered ceramics: in the form of rectangular parallelepiped ($10 \times 2 \times 2$ mm^3) for specific electric conductivity (σ_t) measurements and in the form of disks (diameter 11 mm, thickness 1 mm) for evaluating the ion transport numbers (t_o). The conductivity was measured by the standard four-probe DC method. The procedure for measuring the electric conductivity as a function of oxygen partial pressure and temperature was described in [30]. The ion transport numbers were determined from the impedance spectroscopy data and the electromotive force (EMF) of the concentration cells measured depending on the external load [31]. During the measurements by the modified EMF method [31], the samples were exposed to oxygen partial pressure differentials of 1.0/0.21 and 0.21/0.021 atm at 1023–1223 K. This difference was created by supplying oxygen, air, and air–argon mixture to the platinum electrodes. The experimental technique for determining the transport numbers was described in [15, 31].

RESULTS AND DISCUSSION

According to the XRD data, the synthesized materials were single-phase (Fig. 1) and had a fluorite-like crystal structure with unit cell parameters of 0.5535 and 0.5541 nm for $Ce_{0.5}La_{0.4}Pr_{0.1}O_{2-\delta}$ and $Ce_{0.4}La_{0.4}Pr_{0.2}O_{2-\delta}$, respectively.

Figures 2a and 2b give the isothermal dependences of oxygen nonstoichiometry on $\log p(O_2)$. The obtained $p(O_2)$–T–δ diagrams are typical of Pr- and La-substituted cerium oxides [3, 11–14, 32]. In the oxidation region, an δ increases as $p(O_2)$ decreases due to the reduction of Pr^{4+} to Pr^{3+}:

$$2Pr^{4+} + O^{2-} \leftrightarrow 2Pr^{3+} + V_o + 1/2O_2. \quad (1)$$

In the range $p(O_2) = 10^{-8}$–10^{-10} atm, the curve reaches a plateau corresponding to the complete reduction of praseodymium to Pr^{3+}. Note that an increase in the praseodymium content leads to an increase in δ in the samples and simultaneously to expansion of the range of δ. When $p(O_2)$ decreases further, the mechanism of vacancy formation changes:

$$2Ce^{4+} + O^{2-} \leftrightarrow 2Ce^{3+} + V_o + 1/2O_2. \quad (2)$$

In a moderately reductive medium, there are anomalies at $\delta \approx 0.255$ for $Ce_{0.5}La_{0.4}Pr_{0.1}O_{2-\delta}$ and $\delta \approx 0.305$ for $Ce_{0.4}La_{0.4}Pr_{0.2}O_{2-\delta}$, indicated by arrows in Fig. 2. These inflections are absent in the $p(O_2)$–T–δ diagrams of $Ce_{1-x}Ln_xO_{2-\delta}$ with a doping level of $x \le 40\%$ [3, 11–14, 18, 20, 32]. To examine the possible reasons, the samples were reduced in a 7% H_2–Ar gas mixture at 973 and 1223 K. The diffraction patterns of the reduced samples and the corresponding $p(O_2)$ are shown in Fig. 1. For $Ce_{0.5}La_{0.4}Pr_{0.1}O_{2-\delta}$, there were no changes in the phase composition, whereas for $Ce_{0.4}La_{0.4}Pr_{0.2}O_{2-\delta}$, trace amounts of the C type phase of Ln_2O_3 are observed. It should be emphasized that the reduced Ce_2O_3 also forms a C type phase. Thus, the anomalies of the $p(O_2)$–T–δ diagrams may be related to the segregation of domains with predominant La^{3+}, Pr^{3+}, and Ce^{3+} contents. On the other hand, the content of the C type impurity in reduced $Ce_{0.4}La_{0.4}Pr_{0.2}O_{2-\delta}$ was less than 1% at 973–1223 K. Therefore, the observed anomalies may also indicate the appearance of an additional type of equilibrium of defects associated with the formation of clusters of oxygen vacancies and Ln^{3+} at relatively high oxygen nonstoichiometry.

The changes in the oxygen chemical potential ($\Delta\mu_o$) were determined with the help of the obtained $p(O_2)$–T–δ diagrams:

$$\Delta\mu_o(\delta, T) = \frac{1}{2} RT \ln p(O_2), \quad (3)$$

where R is the gas constant. As $\Delta\mu_o(\delta, T)$ depends linearly on temperature for each composition at fixed δ values, the partial molar enthalpy $\Delta\bar{H}_o(\delta)$ and entropy $\Delta\bar{S}_o(\delta)$ of oxygen introduction in the lattice were calculated by the equation

$$\Delta\mu_o(\delta, T) = \Delta\bar{H}_o(\delta) - T\Delta\bar{S}_o(\delta). \quad (4)$$

The dependences of the partial molar thermodynamic functions of oxygen on δ in $Ce_{0.6-x}La_{0.4}Pr_xO_{2-\delta}$ are shown in Figs. 3a–3d. These dependences are nonmonotonic with two breaks in the function associated with a change in the dominant mechanisms of

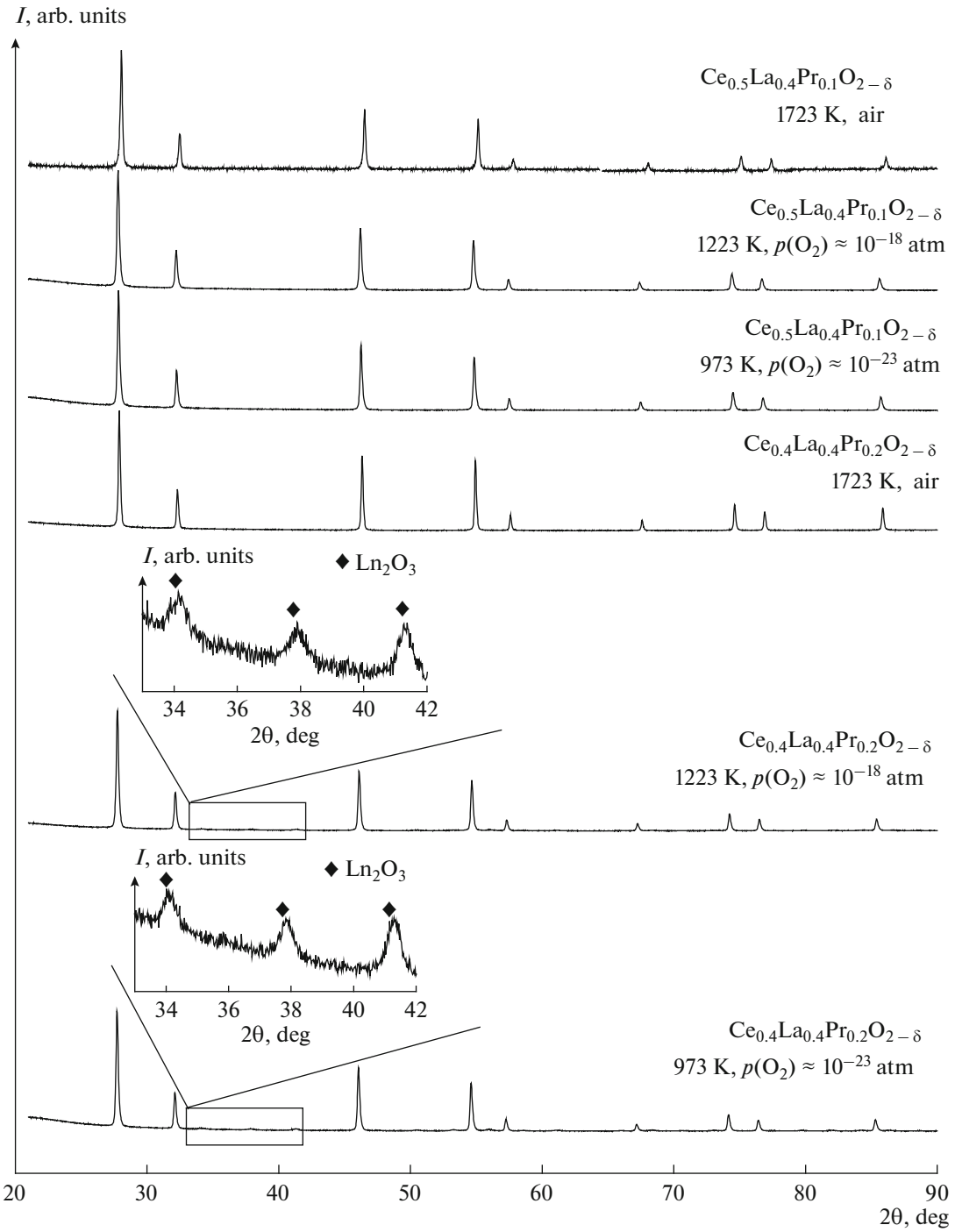

Fig. 1. X-ray diffraction patterns of $Ce_{0.6-x}La_{0.4}Pr_xO_{2-\delta}$ ceramics after sintering in air and annealing in reducing conditions.

defect formation, as discussed above. The observed behavior unambiguously shows that models of an ideal or regular solution are not suitable for describing the processes of intercalation/deintercalation of oxygen. As δ increases in $Ce_{0.5}La_{0.4}Pr_{0.1}O_{2-\delta}$, there is a significant decrease in $\Delta\bar{H}_o$ from –60 to –250 kJ/mol, indicating that the oxygen exit from the lattice becomes increasingly less energetically favorable due to the increase in the binding energy. In the narrow intermediate range $0.250 < \delta < 0.255$, $\Delta\bar{H}_o$ depends but slightly on δ and lies in the range from –275 to –295 kJ/mol. Then $\Delta\bar{H}_o$ increases almost linearly with nonstoichiometry ($\delta > 0.255$). This tendency gives an additional argument in favor of the increase of defective clusters and/or phase transition by the domain mechanism.

For $Ce_{0.4}La_{0.4}Pr_{0.2}O_{2-\delta}$, a section with $0.257 < \delta < 0.280$ can be isolated in the region corresponding to praseodymium reduction, where $\Delta\bar{H}_o$ is almost constant (Fig. 3b). The average $\Delta\bar{H}_o$ value in this range is -108 ± 9 kJ/mol, which coincides well with $\Delta\bar{H}_o$ obtained for $Ce_{0.8}Pr_{0.2}O_{2-\delta}$ at $\delta < 0.1$ within the error [11]. In other ranges of δ in $Ce_{0.4}La_{0.4}Pr_{0.2}O_{2-\delta}$, the tendencies are qualitatively similar to those in $Ce_{0.5}La_{0.4}Pr_{0.1}O_{2-\delta}$. The average value of $\Delta\bar{H}_o = -366 \pm 31$ kJ/mol for $Ce_{0.4}La_{0.4}Pr_{0.2}O_{2-\delta}$ also coincides well with the range of $\Delta\bar{H}_o$ for $Ce_{0.8}Pr_{0.2}O_{2-\delta}$ (-340 ± 7 kJ/mol at $\delta > 0.1$ [11]).

The transport number measurements showed that the $Ce_{0.6-x}La_{0.4}Pr_xO_{2-\delta}$ solid solutions are mixed conductors with a dominant contribution of anion conductivity (Fig. 4). A decrease in temperature leads to a decrease in the ion contribution to electric conductivity, while an increase in the praseodymium concentration leads to a significant increase in the contribution of *p*-type electron conductivity. The latter also becomes apparent when analyzing the isothermal dependences of electric conductivity of $Ce_{0.4}La_{0.4}Pr_{0.2}O_{2-\delta}$ on $p(O_2)$ (Fig. 5). In the oxidation region, the hole contribution provided by the $Pr^{4+/3+}$ redox pair decreases with $p(O_2)$. In the reduction region, the conductivity increases when $p(O_2)$ decreases due to the appearance of *n*-type electron charge carriers owing to the partial reduction of Ce^{4+} to Ce^{3+}. Taking into account the $p(O_2)$–T–δ diagrams, the experimental conductivities were recalculated into dependences of the form $\sigma_t = f(\delta)_T$ shown in Figs. 6a and 6b. The calculations showed that the specific electric conductivity is well described by the standard Arrhenius model at fixed non-stoichiometry values. The activation energy slightly increases with δ and lies in the range 96–128 kJ/mol.

In the reduction and oxidation regions, where the mechanisms of defect formation and transport are relatively simple, the dependence of electric conductivity on nonstoichiometry can be linearized using a simplified model $\sigma_t = \sigma_e + \sigma_i$, where σ_i and σ_e are the partial ion and electron (*p*- or *n*-type) conductivity. Within the framework of this model, it was assumed that the mobilities of electron and ion charge carriers do not depend on their concentration. Then the expression for electric conductivity in the oxidation and reduction regions has the form: $\sigma_t = [Pr^{4+}]k_p + \delta k_i$ and $\sigma_t = [Ce^{3+}]k_n + \delta k_i$, respectively, where $[Pr^{4+}]$ and $[Ce^{3+}]$ are the relative concentrations of holes and electrons localized on the corresponding cations, and k_p, k_n and k_i are constants at a constant temperature. Assuming that the Ce^{3+} concentration is close to zero under the oxidative conditions, the condition of electroneutral crystal lattice can be recorded as $2\delta = [Pr^{3+}] + [La^{3+}]$; in this case, $[Pr^{4+}] + [Pr^{3+}] = x$ and $[La^{3+}] = 0.4$. Similarly, in the reduction region (assuming that praseodymium was completely reduced to Pr^{3+}): $2\delta = [Pr^{3+}] + [La^{3+}] + [Ce^{3+}]$, $[Ce^{4+}] + [Ce^{3+}] = (0.6 - x)$, $[Pr^{3+}] = x$. By combining these equations, we obtain

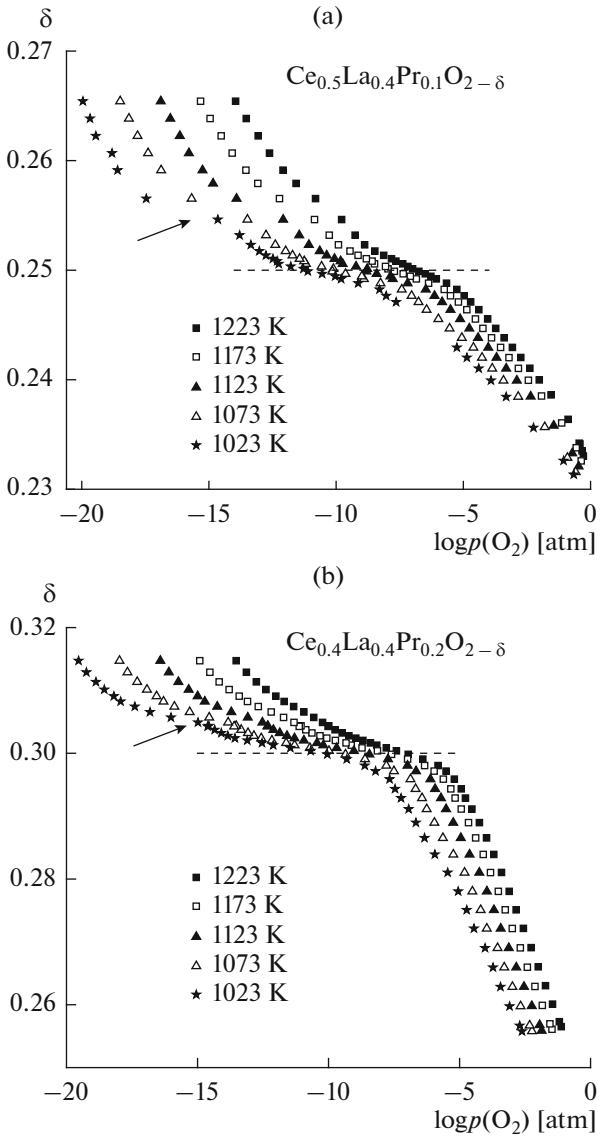

Fig. 2. Dependences of the oxygen nonstoichiometry of $Ce_{0.6-x}La_{0.4}Pr_xO_{2-\delta}$ on the oxygen partial pressure. Dashed line: the δ value corresponding to the complete reduction of praseodymium to Pr^{3+}.

$$\sigma_t = k_p(x - 2\delta + 0.4) + k_i\delta, \quad (5)$$

$$\sigma_t = k_n(2\delta - x - 0.4) + k_i\delta \quad (6)$$

for the oxidation and reduction regions, respectively. The results of the linear regression analysis of the dependences $\sigma_t = f(\delta)_T$ by (5) and (6) are illustrated in Figs. 6a and 6b.

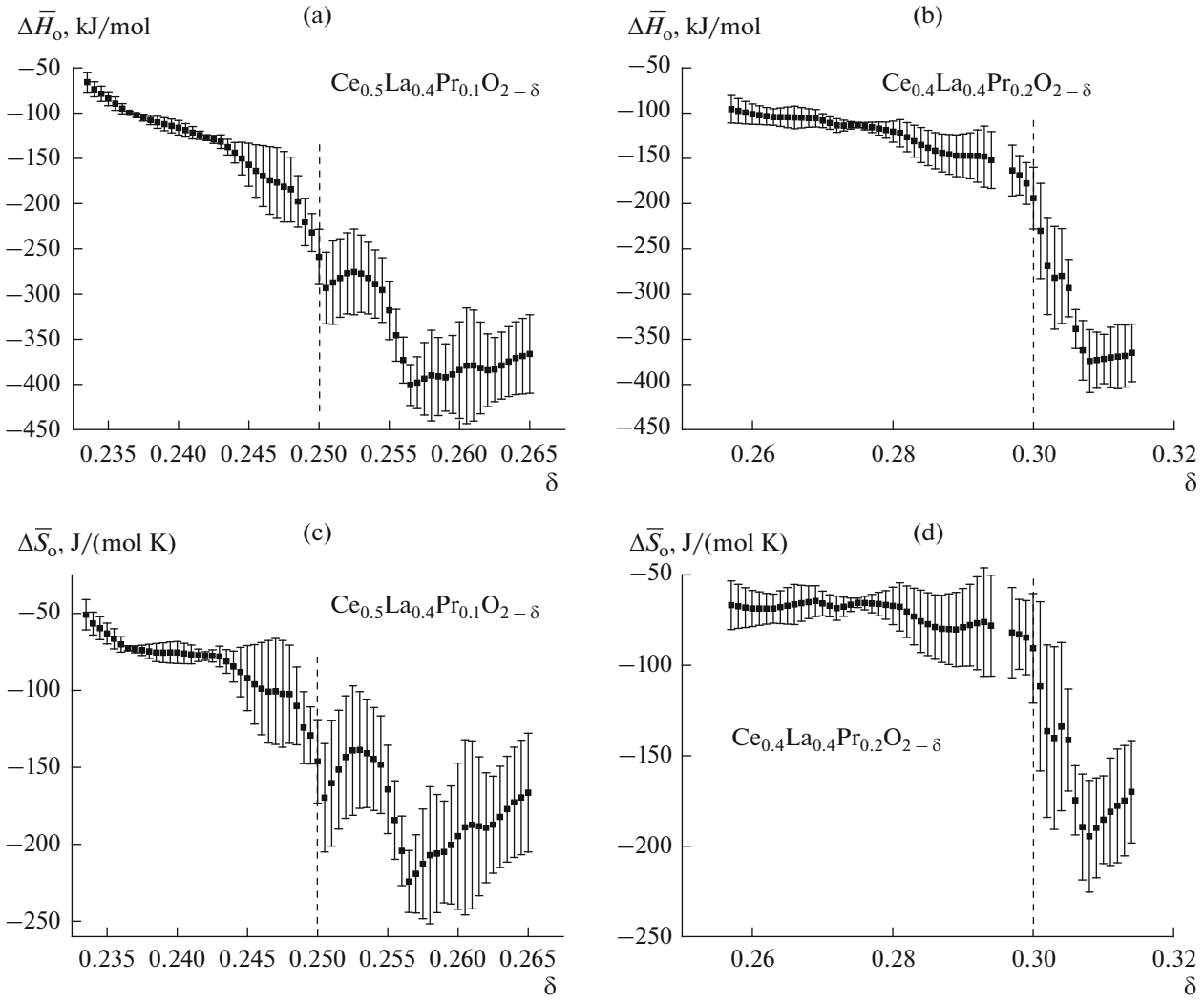

Fig. 3. Dependences of (a and b) the partial molar enthalpies and (c and d) entropies of oxygen on the nonstoichiometry of $Ce_{0.6-x}La_{0.4}Pr_xO_{2-\delta}$.

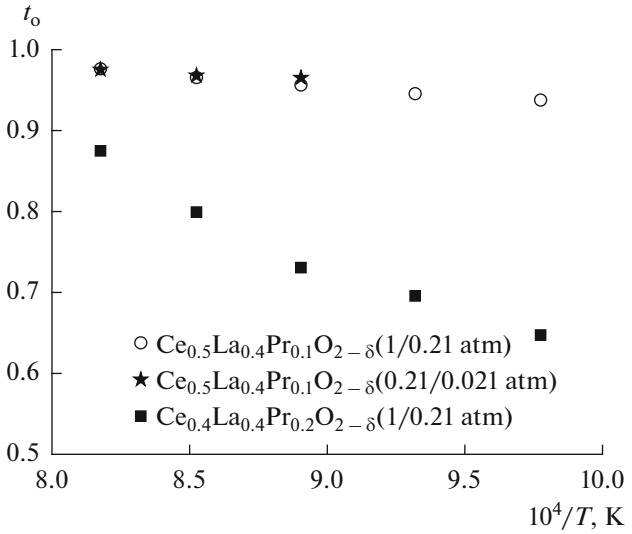

Fig. 4. Oxygen-ion transport numbers of $Ce_{0.6-x}La_{0.4}Pr_xO_{2-\delta}$ measured by the modified EMF method.

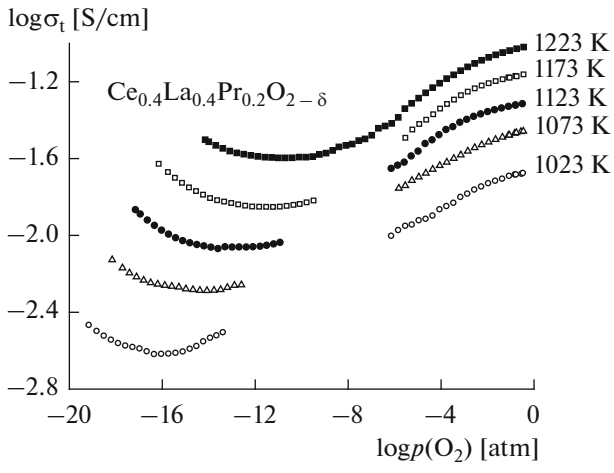

Fig. 5. Dependences of the specific electric conductivity of $Ce_{0.4}La_{0.4}Pr_{0.2}O_{2-\delta}$ on the oxygen partial pressure.

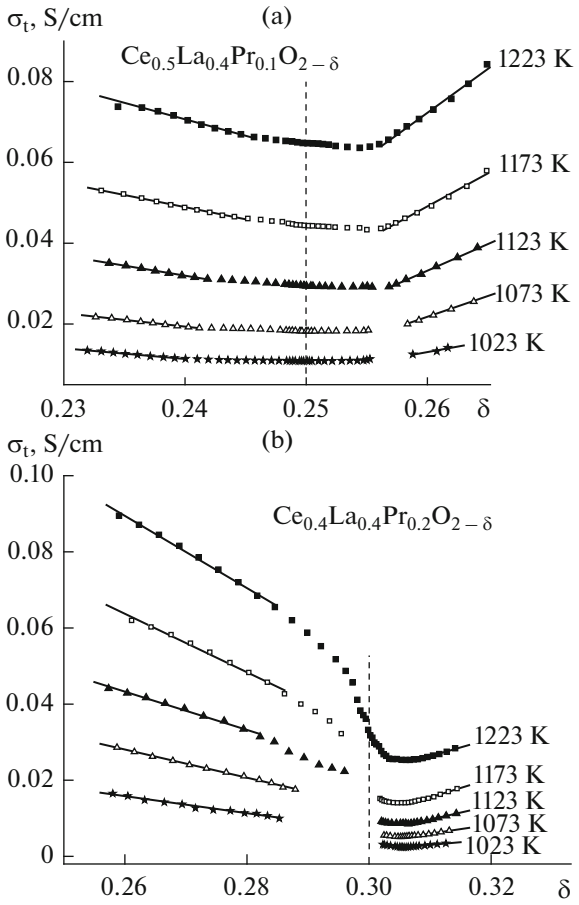

Fig. 6. Dependences of the specific electric conductivity of $Ce_{0.6 - x}La_{0.4}Pr_xO_{2 - \delta}$ on oxygen nonstoichiometry. Straight lines: simplified linear model (Eqs. (5) and (6)).

CONCLUSIONS

The dependences of oxygen nonstoichiometry and specific electric conductivity of fluorite-like solid solutions $Ce_{0.6 - x}La_{0.4}Pr_xO_{2 - \delta}$ ($x = 0.1$–0.2) on the oxygen partial pressure were studied in the range 10^{-19}–0.35 atm at 1023–1223 K. The partial molar thermodynamic functions of intercalation/deintercalation of oxygen from the crystal lattice were evaluated based on the equilibrium $p(O_2)$–T–δ diagrams. It was confirmed that the $Pr^{4+/3+}$ and $Ce^{4+/3+}$ redox pairs play the dominant role in the oxidizing and reducing atmospheres, respectively. These equilibria determine both the concentration of *p*- and *n*-type electron charge carriers and the concentration of oxygen vacancies and hence the ion conductivity. The linear dependences of electric conductivity on nonstoichiometry show that the mobilities of all types of charge carriers are independent or weakly dependent on the carrier concentration. At the same time, the anomalies of the $p(O_2)$–T–δ diagrams and changes in the partial thermodynamic functions of oxygen under moderately reducing conditions indicate the presence of additional processes supposedly associated with the mass formation of clusters formed by oxygen vacancies and trivalent cations or highly nonstoichiometric domains with a *C* type cubic structure. It was found that an increase in the praseodymium concentration leads to a significant increase in the *p* type electric conductivity and expansion of the range of oxygen nonstoichiometry under the oxidizing conditions. In the reducing atmospheres, where the predominant oxidation level of praseodymium cations is 3+, the tendency is the opposite.

ACKNOWLEDGMENTS

This study was financially supported by the Russian Scientific Foundation (project no. 17-79-30071). The experimental techniques and measuring stands used for the study were developed with support from the Ministry of Education and Science of the Russian Federation (contract 14.B25.31.0018).

REFERENCES

1. Kharton, V.V., Figueiredo, F.M., Navarro, L., Naumovich, E.N., Kovalevsky, A.V., Yaremchenko, A.A., Viskup, A.P., Carneiro, A., Marques, F.M.B., and Frade, J.R., Ceria-based materials for solid oxide fuel cells, *J. Mater. Sci.*, 2001, vol. 36, p. 1105.
2. Trovarelli, A., Catalytic properties of ceria and CeO_2-containing materials, *Catal. Rev.*, 2006, vol. 38, p. 439.
3. Mogensen, M., Sammes, N.M., and Tompsett, G.A., Physical, chemical and electrochemical properties of pure and doped ceria, *Solid State Ionics*, 2000, vol. 129, p. 63.
4. Elyassi, B., Rajabbeigi, N., Khodadadi, A., Mohajerzadeh, S.S., and Sahimi, M., An yttria-doped ceria-based oxygen sensor with solid-state reference, *Sens. Actuators, B*, 2004, vol. 103, p. 178.
5. Bernal, S., Blanco, G., Cauqui, M.A., Corchado, M.P., Larese, C., Pintado, J.M., and Rodriguez-Izquierdo, J.M., Cerium–terbium mixed oxides as alternative components for three-way catalysts: a comparative study of $Pt/CeTbO_x$ and Pt/CeO_2 model systems, *Catal. Today*, 1999, vol. 53, p. 607.
6. Zhao, S. and Gorte, R.J., A comparison of ceria and Sm-doped ceria for hydrocarbon oxidation reactions, *Appl. Catal. A*, 2004, vol. 277, p 129.
7. Shuk, P. and Greenblatt, M., Hydrothermal synthesis and properties of mixed conductors based on $Ce_{1 - x}Pr_xO_{2 - \delta}$ solid solutions, *Solid State Ionics*, 1999, vol. 116, p. 217.
8. Ramasamy, D., Shaula, A.L., Gómez-Herrero, A., Kharton, V.V., and Fagg, D.P., Oxygen permeability of mixed-conducting $Ce_{0.8}Tb_{0.2}O_{2 - \delta}$ membranes: Effects of ceramic microstructure and sintering temperature, *J. Membr. Sci.*, 2015, vol. 475, p. 414.
9. Fagg, D.P., Kharton, V.V., Shaula, A., Marozau, I.P., and Frade, J.R., Mixed conductivity, thermal expansion, and oxygen permeability of $Ce(Pr,Zr)O_{2 - \delta}$, *Solid State Ionics*, 2005, vol. 176, p. 1723.

10. Fagg, D.P., Marozau, I.P., Shaula, A.L., Kharton, V.V., and Frade, J.R., Oxygen permeability, thermal expansion and mixed conductivity of $Gd_xCe_{0.8-x}Pr_{0.2}O_{2-\delta}$, $x = 0$, 0.15, 0.2, *J. Solid State Chem.*, 2006, vol. 179, p. 3347.
11. Chatzichristodoulou, C. and Hendriksen, P.V., Oxygen nonstoichiometry and defect chemistry modeling of $Ce_{0.8}Pr_{0.2}O_{2-\delta}$, *J. Electrochem. Soc.*, 2010, vol. 157, p. B481.
12. Bishop, S.R., Stefanik, T.S, and Tuller, H.L., Defects and transport in $Pr_xCe_{1-x}O_{2-\delta}$: Composition trends, *J. Mater. Res.*, 2012, vol. 27, p. 2009.
13. Bishop, S.R., Stefanik, T.S, and Tuller H.L., Electrical conductivity and defect equilibria of $Pr_{0.1}Ce_{0.9}O_{2-\delta}$, *Phys. Chem. Chem. Phys.*, 2011. vol. 13, p. 10165.
14. Fagg, D.P., Frade, J.R., Kharton, V.V., and Marozau, I.P., The defect chemistry of Ce(Pr, Zr)$O_{2-\delta}$, *J. Solid State Chem.*, 2006, vol. 179, p. 1469.
15. Kharton, V.V., Viskup, A.P., Figueiredo, F.M., Naumovich, E.N., Yaremchenko, A.A., and Marques, F.M.B., Electron–hole conduction in Pr-doped Ce(Gd)$O_{2-\delta}$ by faradaic efficiency and emf measurements, *Electrochim. Acta.*, 2001, vol. 46, p. 2879.
16. Schmale, K., Grünebaum, M., Janssen, M., Baumann, S., Schulze-Küppers, F., and Wiemhöfer, H.-D., Electronic conductivity of $Ce_{0.8}Gd_{0.2-x}Pr_xO_{2-\delta}$ and influence of added CoO, *Phys. Status Solidi B*, 2011, vol. 248, p. 314.
17. Ivanov, A.I., Zagitova, A.A., Bredikhin, S.I., and Kharton, V.V., *Sintez i smeshannaya provodimost'* $Ce_{1-x-y}La_xPr_yO_{2-\delta}$ *dlya kataliticheski aktivnykh zashchitnykh podsloev tverdookisnykh toplivnykh elementov*, *Al'tern. Energ. Ekol.,* 2013, no. 20 (160), p. 15.
18. Bishop, S.R., Duncan, K.L., and Wachsman, E.D., Defect equilibria and chemical expansion in non-stoichiometric undoped and gadolinium-doped cerium oxide, *Electrochim. Acta*, 2009, vol. 54, p. 1436.
19. Shoko, E., Smith, M.F., and McKenzie, R.H., Charge distribution and transport properties in reduced ceria phases: A review, *J. Phys. Chem. Solids*, 2011, vol. 72, p. 1482.
20. Otake, T., Yugami, H., Yashiro, K., Nigara, Y., Kawada, T., and Mizusaki, J., Nonstoichiometry of $Ce_{1-x}Y_xO_{2-0.52-\delta}$ ($x = 0.1$, 0.2), *Solid State Ionics*, 2003, vol. 161, p. 181.
21. Naik, I.K. and Tien, T.Y., Small-polaron mobility in nonstoichiometric cerium dioxide, *J. Phys. Chem. Solids*, 1978, vol. 39, p. 311.
22. Tuller, H.L. and Nowick, A.S., Small polaron electron transport in reduced CeO_2 single crystals, *J. Phys. Chem. Solids*, 1978, vol. 38, p. 859.
23. Wei-Ping, G., Rui, Z., and Zhong-Sheng, C., Thermodynamic modelling and applications of Ce–La–O phase diagram, *Trans. Nonferrous Met. Soc. China*, 2011, vol. 21, p. 2671.
24. Wan, J., Goodenough, J.B., and Zhu, J.H., $Nd_{2-x}La_xNiO_{4+\delta}$, a mixed ionic/electronic conductor with interstitial oxygen, as a cathode material, *Solid State Ionics*, 2007, vol. 178, p. 281.
25. Huang, K., Wan, J.-H., and Goodenough, J.B., Increasing power density of LSGM-based solid oxide fuel cells using new anode materials, *J. Electrochem. Soc.*, 2001, vol. 148, p. A788.
26. Wan, J.-H., Yan, J.-Q., and Goodenough, J.B., LSGM-based solid oxide fuel cell with 1.4 W/cm^2 power density and 30 day long-term stability, *J. Electrochem. Soc.*, 2005, vol. 152, p. A1511.
27. Kuritsyna, I., Sinitsyn, V., Melnikov, A., Fedotov, Yu., Tsipis, E., Viskup, A., Bredikhin, S., and Kharton, V., Oxygen exchange, thermochemical expansion and cathodic behavior of perovskite-like $Sr_{0.7}Ce_{0.3}MnO_{3-\delta}$, *Solid State Ionics*, 2014, vol. 262, p. 349.
28. Kuritsyna, I.E., Sinitsyn, V.V., Fedotov, Yu.S., Bredikhin, S.I., Tsipis, E.V., and Kharton, V.V., Stability and functional properties of $Sr_{0.7}Ce_{0.3}MnO_{3-\delta}$ as cathode material for solid oxide fuel cells, *Russ. J. Electrochem.*, 2014, V. 50, p. 713.
29. Patrakeev, M.V., Leonidov, I.A., and Kozhevnikov, V.L., Applications of coulometric titration for studies of oxygen non-stoichiometry in oxides, *J. Solid State Electrochem.*, 2011, vol. 15, p. 931.
30. Patrakeev, M.V., Mitberg, E.B., Lakhtin, A.A., Leonidov, I.A., Kozhevnikov, V.L., Kharton, V.V., Avdeev, M., and Marques, F.M.B., Oxygen nonstoichiometry, conductivity, and Seebeck coefficient of $La_{0.3}Sr_{0.7}Fe_{1-x}Ga_xO_{2.65+\delta}$ perovskites, *J. Solid State Chem.*, 2002, vol. 167, p. 203.
31. Kharton, V.V. and Marques, F.M.B., Interfacial effects in electrochemical cells for oxygen ionic conduction measurements I. The e.m.f. method, *Solid State Ionics*, 2001, vol. 140, p. 381.
32. Sato, H., Hashimoto, S., Nakamura, T., Yashiro, K., Amezawa, K., and Kawada, T., Oxygen nonstoichiometry of $Ce_{0.6}La_{0.4}O_{2-\delta}$, *ECS Trans.*, 2013, vol. 57, p. 1125.

Translated by L. Smolina